Effect of Nonlocal Correlations on the Electronic Structure of LiFeAs

Karim Zantout,[1,*] Steffen Backes,[2] and Roser Valentí[1]
[1]Institut für Theoretische Physik, Goethe-Universität Frankfurt, 60438 Frankfurt am Main, Germany
[2]CPHT, CNRS, Institut Polytechnique de Paris, F-91128 Palaiseau, France

(Received 3 July 2019; published 16 December 2019; corrected 17 November 2020)

We investigate the role of nonlocal correlations in LiFeAs by exploring an *ab initio*–derived multiorbital Hubbard model for LiFeAs via the two-particle self-consistent (TPSC) approach. The multiorbital formulation of TPSC approximates the irreducible interaction vertex to be an orbital-dependent constant, which is self-consistently determined from local spin and charge sum rules. Within this approach, we disentangle the contribution of local and nonlocal correlations in LiFeAs and show that in the local approximation one recovers the dynamical mean field theory result. The comparison of our theoretical results to most recent angular-resolved photoemission spectroscopy and de Haas–van Alphen data shows that nonlocal correlations in LiFeAs are decisive to describe the measured spectral function $A(\vec{k},\omega)$, Fermi surface, and scattering rates. These findings underline the importance of nonlocal correlations and benchmark different theoretical approaches for iron-based superconductors.

DOI: 10.1103/PhysRevLett.123.256401

Introduction.—The nature of the electronic structure in iron-based superconductors has been intensely scrutinized since their discovery in 2008 [1,2]. While *ab initio* density functional theory (DFT) calculations can provide a qualitative understanding of their band structure and Fermi surface [3–5], it soon became evident that correlation effects originating from the strong local Coulomb repulsion on the Fe atoms are responsible for many experimental findings such as large effective masses, Fermi surface renormalization, finite lifetimes, or transfer of spectral weight to high binding energies [6–20]. The combined DFT with dynamical mean field theory (DFT + DMFT) method, which approximates the electronic self-energy to be local in space and thus includes frequency- and orbital-dependent local effects of electronic correlations, has been very successful in capturing many of these observations. Some examples are orbital-dependent correlations, incoherence properties, and Fermi surface renormalization [10–18,20–22]. However, the single-site DMFT cannot account for possible momentum-dependent correlation effects such as relative band shifts in opposite directions of, respectively, hole bands centered at Γ and electron bands centered at the Brillouin zone edge M (the so-called "blueshift-redshift") in a large class of iron-based superconductors [23–27], or the recently reported [28] possible momentum-dependent scattering rates in angular-resolved photoemission spectroscopy (ARPES) measurements of LiFeAs. Some of these effects have been suggested to play an important role in the superconducting pairing mechanism [24,29–31] as well.

Consideration of momentum dependence in the self-energy in real materials' calculations are scarce but promising [32–38], showing, for instance, effects of bandwidth widening and momentum-dependent band shifts in the systems studied [33,35,37]. Here we explore this dependence by considering an approach where spin fluctuations play the dominant role and it allows both a description of local and nonlocal correlations on an equal footing.

The purpose of this work is twofold. (i) We first introduce the multiorbital formulation of the two-particle self-consistent (TPSC) approach originally conceived for the single-orbital Hubbard model [39], which provides momentum- and frequency- dependent self-energies in the intermediate coupling regime. (ii) We apply the method to the iron-based superconductor LiFeAs.

We find that the momentum dependence obtained within the TPSC approach introduces drastic changes to the LiFeAs Fermi surface and band structure with respect to DFT results. First, the innermost hole pocket centered at Γ is shifted below the Fermi energy E_F as de Haas–van Alphen (dHvA) and ARPES [26,40] measurements already suggested. Second, we find a large accumulation of incoherent spectral weight around the Γ point, as observed in ARPES [24–26,28,30]. Third, the relative blueshift-redshift of the bands centered at Γ and M, respectively [24,25], is properly described. Fourth, the momentum-averaged TPSC results agree with the results obtained from previous local DFT + DMFT calculations [15,25] pointing to an important relation between both approaches in this region of interactions.

Models and methods.—Starting from a DFT calculation of LiFeAs in the tetragonal crystal structure [41] within the generalized gradient approximation (GGA) [42] using the full-potential linear augmented plane-wave basis from WIEN2k [43], we derive an effective low-energy model

 © 2019 American Physical Society

comprising the Fe $3d$ orbitals using maximally localized Wannier functions as implemented in Wannier90 [44] (see Supplemental Material [45]). We effectively then solve a two-dimensional system by restricting our calculation to the $k_z = 0$ plane, since the low-energy electronic structure shows only weak dispersion along k_z. In this Wannier-projected 2D model we have an electron occupation of 6. Interaction parameters for the lattice Hubbard model were obtained within the constrained random-phase approximation [49] on the DFT band structure (see Supplemental Material [45]).

The TPSC method considers the Luttinger-Ward functional $\Phi[G]$ [50,51], which is a functional of the interacting Green's function G and yields the self-energy Σ and two-particle irreducible four-point vertex Γ as functional derivatives:

$$\Sigma = \frac{\delta\Phi}{\delta G}, \qquad \Gamma = \frac{\delta^2\Phi}{\delta G^2}. \tag{1}$$

Within the TPSC approach one approximates the vertex Γ to be static and momentum independent [39] (but fully orbital dependent). One obtains a set of self-consistent and conserving equations that satisfy the Pauli principle and Mermin-Wagner theorem. The range of validity of TPSC is the regime of weak to intermediate couplings where the local and static approximation of the vertex is valid, i.e., away from any phase transition. This method has been extended to multisite [52–57], nearest-neighbor interaction [58], and multiorbital [59] generalizations of the Hubbard model and has provided valuable insight on the pseudogap physics in the cuprates [60] and unconventional superconductivity [54,61,62].

In the multiorbital generalization of the TPSC method, similar to the original formulation [59], we first introduce the noninteracting susceptibility χ^0 given by

$$\chi^0_{\lambda\mu\nu\xi}(\vec{q}, iq_m) = [G^0_{\nu\lambda} \star G^0_{\mu\xi}](\vec{q}, iq_m), \tag{2}$$

where G^0 denotes the noninteracting Green's function in orbital space, $\star$ denotes a convolution over frequency and momentum, and $q_m = 2m\pi T$ is the mth bosonic Matsubara frequency. The interacting susceptibility χ is decomposed into the spin and charge channel (χ^{sp} and χ^{ch}, respectively) and reads

$$\begin{aligned}
\chi^{\mathrm{sp}}(\vec{q}, iq_m) &= [\mathbb{I} - \chi^0(\vec{q}, iq_m)U^{\mathrm{sp}}]^{-1} 2\chi^0(\vec{q}, iq_m), \\
\chi^{\mathrm{ch}}(\vec{q}, iq_m) &= [\mathbb{I} + \chi^0(\vec{q}, iq_m)U^{\mathrm{ch}}]^{-1} 2\chi^0(\vec{q}, iq_m),
\end{aligned} \tag{3}$$

where the inversion of a four-index tensor is given as the matrix inverse after combining the first and last two indices of $\lambda\mu\nu\xi$ into a superindex $(\lambda\mu)(\nu\xi)$.

We only consider the $U^{\mathrm{ch/sp}}_{\alpha\alpha\beta\beta}$ and $U^{\mathrm{ch/sp}}_{\alpha\beta\alpha\beta} = U^{\mathrm{ch/sp}}_{\alpha\beta\beta\alpha}$ matrix elements of the renormalized irreducible vertices in the spin U^{sp} and the charge channel U^{ch} to be nonzero, corresponding to the atomic symmetry of $3d$ orbitals. Those elements are determined by enforcing the following local spin and charge sum rules:

$$\begin{aligned}
&\frac{T}{N_{\vec{q}}}\sum_{\vec{q},m} \chi^{\mathrm{sp}}_{\mu\mu\mu\mu}(\vec{q}, iq_m) = \langle n_{\mu\uparrow}\rangle + \langle n_{\nu\uparrow}\rangle - 2\langle n_{\mu\uparrow} n_{\nu\downarrow}\rangle, \\
&\frac{T}{N_{\vec{q}}}\sum_{\vec{q},m} \chi^{\mathrm{sp}}_{\mu\mu\nu\nu}(\vec{q}, iq_m) \overset{\mu\neq\nu}{=} 2\langle n_{\mu\uparrow} n_{\nu\uparrow}\rangle - 2\langle n_{\mu\uparrow} n_{\nu\downarrow}\rangle, \\
&\frac{T}{N_{\vec{q}}}\sum_{\vec{q},m} \chi^{\mathrm{ch}}_{\mu\mu\nu\nu}(\vec{q}, iq_m) = 2\langle (n_{\mu\uparrow} + n_{\mu\downarrow}) n_{\nu\uparrow}\rangle - n_\mu n_\nu, \\
&\frac{T}{N_{\vec{q}}}\sum_{\vec{q},m} \chi^{\mathrm{ch}}_{\mu\nu\mu\nu}(\vec{q}, iq_m) \overset{\mu\neq\nu}{=} \frac{n_\mu + n_\nu}{2} - \langle (4n_{\mu\uparrow} - 2n_{\mu\downarrow}) n_{\nu\uparrow}\rangle.
\end{aligned} \tag{4}$$

In order to solve this underdetermined set of equations, we employ an ansatz for the spin vertex U^{sp} that is motivated by the Kanamori-Brueckner screening [39,59] and introduce an additional particle-hole symmetrization to keep all equations within TPSC particle-hole symmetric:

$$\begin{aligned}
U^{\mathrm{sp}}_{\mu\mu\mu\mu} &= \frac{1}{2}\left(\frac{\langle n_{\mu\uparrow} n_{\mu\downarrow}\rangle}{\langle n_{\mu\uparrow}\rangle\langle n_{\mu\downarrow}\rangle} + \text{particle} \leftrightarrow \text{hole}\right) U_{\mu\mu}, \\
U^{\mathrm{sp}}_{\mu\nu\mu\nu} &= \frac{1}{2}\left[\frac{\langle n_{\mu\uparrow} n_{\nu\downarrow}\rangle}{\langle n_{\mu\uparrow}\rangle\langle n_{\nu\downarrow}\rangle} U_{\mu\nu} + \frac{\langle n_{\mu\uparrow} n_{\nu\uparrow}\rangle}{\langle n_{\mu\uparrow}\rangle\langle n_{\nu\uparrow}\rangle}(U_{\mu\nu} - J_{\mu\nu})\right. \\
&\qquad \left. + \text{particle} \leftrightarrow \text{hole}\right] = U^{\mathrm{sp}}_{\mu\mu\nu\nu} = U^{\mathrm{sp}}_{\mu\nu\nu\mu}.
\end{aligned} \tag{5}$$

The local spin vertex U^{sp} can be obtained by iterating the equations above. For the charge channel we optimize U^{ch} in order to fulfill the corresponding charge sum rules, restricting to positive values of U^{ch} because in certain cases negative values can lead to noncausal self-energies. Because of the constraint we search for values of U^{ch} that minimize (see Supplemental Material [45]) the difference between the left-hand side and right-hand side of the charge sum rules [Eq. (4)].

After the determination of the spin and charge vertices, the self-energy Σ and interacting Green's function G are then given as

$$\begin{aligned}
\Sigma_{\mu\nu} &= \frac{1}{4}\sum_{\alpha,\beta} \underbrace{[U^{\mathrm{sp}}\chi^{\mathrm{sp}}U^{\mathrm{sp},0} + U^{\mathrm{ch}}\chi^{\mathrm{ch}}U^{\mathrm{ch},0}]_{\nu\alpha\mu\beta}}_{:=V_{\nu\alpha\mu\beta}} \star G^0_{\beta\alpha}, \\
G(\vec{k}, i\omega_n) &= [(i\omega_n + \mu)\mathbb{I} - H_0(\vec{k}) - \Sigma(\vec{k}, i\omega_n)]^{-1},
\end{aligned} \tag{6}$$

where the noninteracting vertices are zero except for the matrix elements: $U^{\mathrm{sp/ch},0}_{\mu\mu\mu\mu} = U_{\mu\mu}$, $U^{\mathrm{ch},0}_{\mu\mu\nu\nu} = 2U_{\mu\nu} - J_{\mu\nu}$, and $U^{\mathrm{sp/ch},0}_{\mu\nu\mu\nu} = U^{\mathrm{sp/ch},0}_{\mu\nu\nu\mu} = U^{\mathrm{sp},0}_{\mu\mu\nu\nu} = J_{\mu\nu}$, with $\mu \neq \nu$. No Hartree term is included in Σ since it is already contained in the DFT-derived Hamiltonian H_0.

Our multiorbital extension of TPSC differs from previous formulations [59] on the following aspects. It restricts the self-consistent equations in the charge channel in Eq. (3) to ensure positivity of the spectral weight and chooses a symmetrized ansatz for U^{sp} [Eq. (5)]. Furthermore, the set of local spin and charge sum rules [Eq. (4)] and bare vertex tensors $U^{\mathrm{ch},0}$, $U^{\mathrm{sp},0}$ [Eq. (6)] and their dependence on U, J are derived from the Bethe-Salpeter equation for the self-energy Σ within TPSC [39], which is different from the random-phase approximation derived expression of $U^{\mathrm{ch},0}$, $U^{\mathrm{sp},0}$ only in the $ijij$ element, $i \neq j$ [59].

Our calculations were performed at $T = 0.015$ eV $\approx$ 174 K since this is the lowest accessible temperature before spin fluctuations get too strong and the TPSC approximation is not justified anymore. Nevertheless, we checked that the results presented below do not change in their trends up to room temperature (see Supplemental Material [45]).

Results and discussion.—In Fig. 1 we show the TPSC spectral function $A(\vec{k},\omega)$ for LiFeAs along Γ-X-M-Γ in the two-iron Brillouin zone. To emphasize the changes in the electronic structure beyond an overall bandwidth renormalization of about a factor of 2, we also plot the renormalized DFT band structure on top. We observe that the electronic correlations introduce a down-shift of the hole states around the Fermi level at the Γ point, while the electron states at M are slightly shifted up in energy, the inner electron pocket being shifted by -0.1 eV on average while the outer electron pocket is shifted by only -0.01 eV. This leads to an overall shrinking of hole and electron pockets, corresponding to the blueshift-redshift seen in ARPES measurements [24,26] compared to the DFT band structure. Apart from orbital dependence, the shrinkings are

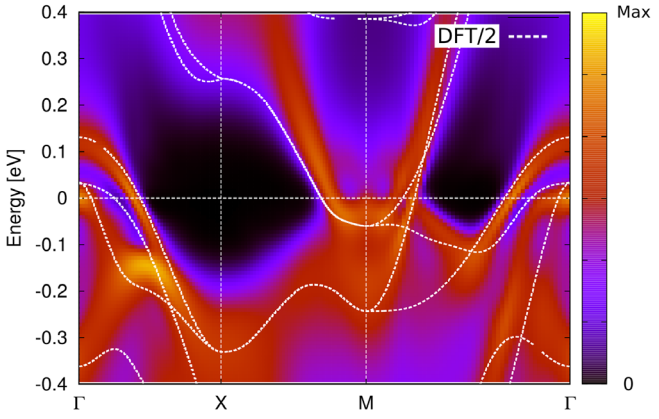

FIG. 1. Interacting spectral function $A(\vec{k},\omega)$ within the TPSC approach for LiFeAs in the two-iron Brillouin zone. For comparison, we show the DFT (GGA) band structure renormalized by the average mass enhancement $\approx$2 (dotted lines). We observe an overall shrinking of the electron and hole pockets at Γ and M originating from the nonlocal components of the self-energy. The center hole pockets at Γ become incoherent and diffuse due to finite lifetime effects in the Fe $3d_{xz}/3d_{yz}$ orbitals.

momentum dependent. For example, along Γ-X the middle hole pocket shrinks to approximately 20% of its size compared to the renormalized DFT band structure while all other parts of the Fermi surface shrink to 80%–90% of their original size. The inner hole pocket at Γ, composed of Fe $3d_{xz}/3d_{yz}$ orbital character [see Fig. 2(a)], becomes very diffuse at the Fermi level due to incoherent scattering processes, leading to a significant reduction of the lifetime of quasiparticle excitations. This manifests in a broad Fermi surface feature very similar to the one observed in ARPES [24–26,28,30]. The maximum of the spectral function of the two inner hole pockets at Γ is shifted basically on top of the Fermi level but retains significant spectral weight at higher and lower binding energies—the shift being on average 0.18 eV for both while for the outer hole pocket it is 0.1 eV. We expect that the inclusion of spin-orbit coupling, which is beyond our current approach, will split this feature, effectively pushing one hole band below and the other above the Fermi level, giving rise to only one central hole Fermi surface pocket, which would be in very good agreement with previous ARPES data [26,63] as well as dHvA experiments [40].

We can trace back these Fermi surface modifications to the value of the self-energy at the specific $\vec{k}$ points in the Brillouin zone: The largest contribution to the diagonal elements of the self-energy in Eq. (6) stems from V_{abab}, which is peaked at $\vec{k} = \{(\pm\pi, 0), (0, \pm\pi)\}$. Following the argumentation of Ref. [23], this leads to a negative (positive) real part of the self-energy in the vicinity of the hole (electron) pockets and thus to the observed blueshift-redshift, and therefore it is a consequence of nonlocal spin fluctuations.

In Fig. 2 we show the orbitally resolved Fermi surface obtained from DFT (within GGA) [Fig. 2(a)], DFT + TPSC [Fig. 2(b)], and DFT+"local TPSC," where the momentum-dependent TPSC self-energy $\Sigma(\vec{k},\omega)$ has been approximated by its local component $(1/N_{\vec{k}})\sum_{\vec{k}}\Sigma(\vec{k},\omega)$ [Fig. 2(c)]. The DFT Fermi surface reveals three well-defined distinct hole pockets centered at Γ with circular to square shape and two electron pockets centered at M. As can already be deduced from the spectral function $A(\vec{k},\omega)$ in Fig. 1, the Fermi surface experiences appreciable changes due to the TPSC self-energy contributions. All pockets are reduced in size, with the remaining spectral weight of the two center hole pockets of Fe $3d_{xz}/3d_{yz}$ character at Γ becoming incoherent and forming a flower-like shape, while the outer hole pocket of $3d_{xy}$ character stays coherent, as confirmed in ARPES measurements [24,26]. The electron pockets at M shrink slightly and broaden, since they are mostly composed of the most incoherent $3d_{xz}/3d_{yz}$ as well.

The observed shrinking of the hole and electron pockets deviates significantly from published DFT + DMFT results, most likely due to the inclusion of nonlocal

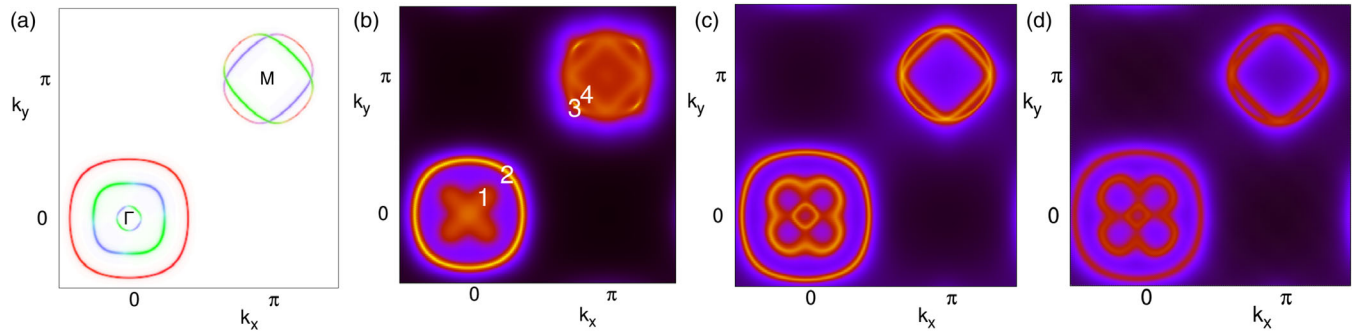

FIG. 2. (a) Orbital-resolved Fermi surface obtained from DFT (GGA) where the dominant orbital characters are d_{xy} (red), d_{yz} (blue), and d_{xz} (green). Three hole pockets are centered around Γ and two electron pockets around the M point. (b) Fermi surface from DFT + TPSC. We observe strong incoherence effects on the inner hole and electron pockets. The two inner hole pockets become very incoherent and form a flowerlike shaped region of spectral weight. (c) Fermi surface from DFT+"local TPSC," where the momentum-dependent TPSC self-energy $\Sigma(\vec{k},\omega)$ has been approximated by its local component $(1/N_{\vec{k}})\sum_{\vec{k}}\Sigma(\vec{k},\omega)$. In this approximation the Fermi surface recovers published DFT + DMFT results well [15,25]. (d) DFT + DMFT Fermi surface for the same model (see Supplemental Material [45]) as used in this work. We see a strong similarity to the DFT + local TPSC result in (c).

correlations in the TPSC approach which go beyond the DMFT approximation where the self-energy is purely local. In order to confirm this assumption, we separate the local from the nonlocal correlation effects by employing a DMFT-like approximation on the TPSC self-energy. We approximate the full momentum-dependent TPSC self-energy $\Sigma(\vec{k},\omega)$ by its local component and compare the resulting Fermi surface to the full result in Fig. 2(c). The so-obtained Fermi surface indeed recovers the result obtained within published DFT + DMFT [15,25], and, when considering the DFT + DMFT results for the same model as used in this work (see Supplemental Material [45]), the agreement is almost perfect [compare Figs. 2(c) and 2(d)]. DFT + DMFT calculations with a different double counting scheme [22] see a more pronounced—although coherent—flowerlike shape of spectral weight around Γ but do not account for the blueshift-redshift. This shows that when taking into account nonlocal fluctuations, the local Coulomb interaction gives rise to a significant momentum-dependent self-energy and can account for the experimentally observed blueshift-redshift. Interestingly, within the local approximation (local TPSC) the center hole pockets at Γ become again coherent, which is also in correspondence with the DMFT result. This shows that the quasiparticle scattering rate itself is strongly momentum and orbital dependent, which has in fact been observed in recent ARPES experiments [26,28], where the inner $3d_{xz}/3d_{yz}$ derived hole Fermi surfaces have been found to be incoherent while the outer $3d_{xy}$ hole pocket shows Fermi-liquid behavior.

Since Fermi-liquid theory predicts a quadratic energy dependence of quasiparticles' lifetimes near the Fermi energy, deviations from this energy dependence are also a signature for non-Fermi-liquid behavior. It is therefore compelling to analyze the energy dependencies of the scattering rate within the TPSC approach. For this, we present the quasiparticle lifetime $-Z_{\vec{k}}\Sigma''(\vec{k},w)$ with

$$Z_{\vec{k}} = \frac{1}{1 - \frac{\partial\Sigma''(\vec{k},i\omega_n)}{\partial w_n}|_{i\omega_n\to 0^+}} \tag{7}$$

in Fig. 3 at four different $\vec{k}$ points in momentum space following the Γ-M path. Along this path the dominating contributions are (1) d_{yz} hole pocket, (2) d_{xy} hole pocket, (3) d_{xy} electron pocket, and (4) d_{xz} electron pocket [see Figs. 2(a) and 2(b)]. The energy dependence of the quasiparticle lifetimes for the $d_{xz/yz}$ electron and hole pockets (red symbols in Fig. 3) are in good agreement with the results of Ref. [26] with values between 0.025 and 0.035 eV. The energy dependence shows a very shallow linear behavior (fitted slopes are of the order of 10^{-3}, see Supplemental Material [45]) similar to the measurements

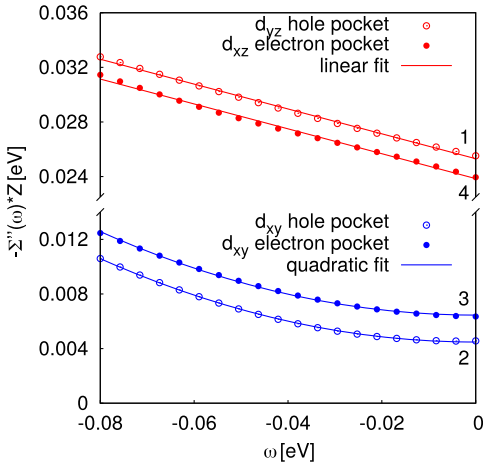

FIG. 3. Quasiparticle lifetimes $-Z_{\vec{k}}\Sigma''(\vec{k},\omega)$ along Γ-M as a function of the binding energy ω [numbers on the right correspond to positions in Fig. 2(c)]. We find that the quasiparticles with $d_{xz/yz}$ character display a linear dependence in ω while the electron pockets have a quadratic increase with energy (see Supplemental Material [45]).

from Ref. [26]. The quasiparticle lifetimes of the d_{xy} hole and electron pockets (blue symbols in Fig. 3), in contrast, show at the considered k points a quadratic increase in energy as in the ARPES measurements of Ref. [26], suggesting a Fermi-liquid-like behavior. Although our data were obtained at $T \approx 174$ K in contrast to the $T = 25$ K in Ref. [26], we are confident that our results are still valid at low temperatures, since, for example, in $Ba(Fe_{0.92}Co_{0.08})_2As_2$ it has been found that the quasiparticle lifetimes for the hole $d_{xz/yz}$ orbitals showed weak temperature dependence. We also checked how these results depend on the $\vec{k}$ path and found that small translations along the tip of electron pocket (3) reveal a linear dependence of the quasiparticle lifetime, as can already be expected since the quasiparticle weight gets incoherent away from the point (3) [see Fig. 2(b)].

Summary.—In conclusion, we presented a multiorbital TPSC scheme that respects local spin and charge sum rules. This method includes effects of local and nonlocal correlations on an equal footing within the validity of the local approximation of the irreducible four-point vertex and thus yields momentum- and frequency-dependent self-energies. We applied this method to the multiorbital iron-based superconductor LiFeAs and found that the nonlocal components of the self-energy are decisive to explain its experimentally observed spectral function $A(k, \omega)$ and Fermi surface. Taking into account nonlocal correlations, we observe a blueshift-redshift of the electronic structure, where the hole bands at the Brillouin zone center are lowered in energy, while the electron bands in the corner of the Brillouin zone are slightly shifted upwards, resulting in an overall reduction of the size of the Fermi surface pockets. Overall, we find very good agreement with ARPES and dHvA experiments, where the blueshift-redshift was first observed. We could show that our TPSC approach within a local approximation to the self-energy recovers the DFT + DMFT result which does not exhibit the blueshift-redshift, both benchmarking the TPSC result and showing the importance of going beyond the local picture of DMFT in order to understand the electronic structure of iron-based superconductors. Furthermore, we also found a strong momentum and nonquadratic energy dependence of the electronic scattering rate, in good agreement with recent ARPES measurements.

This work was supported by the German Research Foundation (Deutsche Forschungsgemeinschaft) under Grant No. SFB/TR 49. We would like to thank S. Bhattacharyya, S. Borisenko, V. Borisov, J. Fink, P. J. Hirschfeld, G. Kotliar, and Y. Li for discussions. R. V. acknowledges the KITP for hospitality where aspects of this work were discussed. The research at KITP was supported in part by NSF Grant No. PHY-1748958.

*zantout@itp.uni-frankfurt.de

[1] Y. Kamihara, T. Watanabe, M. Hirano, and H. Hosono, J. Am. Chem. Soc. **130**, 3296 (2008).
[2] M. Rotter, M. Tegel, and D. Johrendt, Phys. Rev. Lett. **101**, 107006 (2008).
[3] S. Lebègue, Phys. Rev. B **75**, 035110 (2007).
[4] D. J. Singh and M.-H. Du, Phys. Rev. Lett. **100**, 237003 (2008).
[5] I. I. Mazin, M. D. Johannes, L. Boeri, K. Koepernik, and D. J. Singh, Phys. Rev. B **78**, 085104 (2008).
[6] C. Cao, P. J. Hirschfeld, and H.-P. Cheng, Phys. Rev. B **77**, 220506(R) (2008).
[7] Q. Si and E. Abrahams, Phys. Rev. Lett. **101**, 076401 (2008).
[8] M. M. Qazilbash, J. J. Hamlin, R. E. Baumbach, L. Zhang, D. J. Singh, M. B. Maple, and D. N. Basov, Nat. Phys. **5**, 647 (2009).
[9] F. Rullier-Albenque, D. Colson, A. Forget, and H. Alloul, Phys. Rev. Lett. **103**, 057001 (2009).
[10] K. Haule and G. Kotliar, New J. Phys. **11**, 025021 (2009).
[11] L. de' Medici, S. R. Hassan, M. Capone, and X. Dai, Phys. Rev. Lett. **102**, 126401 (2009).
[12] M. Aichhorn, S. Biermann, T. Miyake, A. Georges, and M. Imada, Phys. Rev. B **82**, 064504 (2010).
[13] P. Hansmann, R. Arita, A. Toschi, S. Sakai, G. Sangiovanni, and K. Held, Phys. Rev. Lett. **104**, 197002 (2010).
[14] Z. P. Yin, K. Haule, and G. Kotliar, Nat. Mater. **10**, 932 (2011).
[15] J. Ferber, K. Foyevtsova, R. Valentí, and H. O. Jeschke, Phys. Rev. B **85**, 094505 (2012).
[16] P. Werner, M. Casula, T. Miyake, F. Aryasetiawan, A. J. Millis, and S. Biermann, Nat. Phys. **8**, 331 (2012).
[17] J. Ferber, H. O. Jeschke, and R. Valentí, Phys. Rev. Lett. **109**, 236403 (2012).
[18] D. V. Evtushinsky, M. Aichhorn, Y. Sassa, Z.-H. Liu, J. Maletz, T. Wolf, A. N. Yaresko, S. Biermann, S. V. Borisenko, and B. Büchner, arXiv:1612.02313.
[19] E. Bascones, B. Valenzuela, and M. J. Calderón, C.R. Phys. **17**, 36 (2016).
[20] M. D. Watson, S. Backes, A. A. Haghighirad, M. Hoesch, T. K. Kim, A. I. Coldea, and R. Valentí, Phys. Rev. B **95**, 081106(R) (2017).
[21] H. Miao, Z. P. Yin, S. F. Wu, J. M. Li, J. Ma, B.-Q. Lv, X. P. Wang, T. Qian, P. Richard, L.-Y. Xing, X.-C. Wang, C. Q. Jin, K. Haule, G. Kotliar, and H. Ding, Phys. Rev. B **94**, 201109(R) (2016).
[22] R. Nourafkan, G. Kotliar, and A.-M. S. Tremblay, Phys. Rev. Lett. **117**, 137001 (2016).
[23] L. Ortenzi, E. Cappelluti, L. Benfatto, and L. Pietronero, Phys. Rev. Lett. **103**, 046404 (2009).
[24] S. V. Borisenko, V. B. Zabolotnyy, D. V. Evtushinsky, T. K. Kim, I. V. Morozov, A. N. Yaresko, A. A. Kordyuk, G. Behr, A. Vasiliev, R. Follath, and B. Büchner, Phys. Rev. Lett. **105**, 067002 (2010).
[25] G. Lee, H. S. Ji, Y. Kim, C. Kim, K. Haule, G. Kotliar, B. Lee, S. Khim, K. H. Kim, K. S. Kim, K.-S. Kim, and J. H. Shim, Phys. Rev. Lett. **109**, 177001 (2012).
[26] V. Brouet, D. LeBoeuf, P.-H. Lin, J. Mansart, A. Taleb-Ibrahimi, P. Le Fèvre, F. Bertran, A. Forget, and D. Colson, Phys. Rev. B **93**, 085137 (2016).
[27] Y. S. Kushnirenko, A. A. Kordyuk, A. V. Fedorov, E. Haubold, T. Wolf, B. Büchner, and S. V. Borisenko, Phys. Rev. B **96**, 100504(R) (2017).

[28] J. Fink, J. Nayak, E. D. L. Rienks, J. Bannies, S. Wurmehl, S. Aswartham, I. Morozov, R. Kappenberger, M. A. ElGhazali, L. Craco, H. Rosner, C. Felser, and B. Büchner, Phys. Rev. B **99**, 245156 (2019).
[29] Y. Wang, A. Kreisel, V. B. Zabolotnyy, S. V. Borisenko, B. Büchner, T. A. Maier, P. J. Hirschfeld, and D. J. Scalapino, Phys. Rev. B **88**, 174516 (2013).
[30] H. Miao, T. Qian, X. Shi, P. Richard, T. K. Kim, M. Hoesch, L. Y. Xing, X.-C. Wang, C.-Q. Jin, J.-P. Hu, and H. Ding, Nat. Commun. **6**, 6056 (2015).
[31] D. Altenfeld, P. J. Hirschfeld, I. I. Mazin, and I. Eremin, Phys. Rev. B **97**, 054519 (2018).
[32] S. Biermann, F. Aryasetiawan, and A. Georges, Phys. Rev. Lett. **90**, 086402 (2003).
[33] J. M. Tomczak, M. van Schilfgaarde, and G. Kotliar, Phys. Rev. Lett. **109**, 237010 (2012).
[34] J. M. Tomczak, M. Casula, T. Miyake, and S. Biermann, Phys. Rev. B **90**, 165138 (2014).
[35] A. van Roekeghem, T. Ayral, J. M. Tomczak, M. Casula, N. Xu, H. Ding, M. Ferrero, O. Parcollet, H. Jiang, and S. Biermann, Phys. Rev. Lett. **113**, 266403 (2014).
[36] S. Biermann, J. Phys. Condens. Matter **26**, 173202 (2014).
[37] S. Li, N. Kaushal, Y. Wang, Y. Tang, G. Alvarez, A. Nocera, T. A. Maier, E. Dagotto, and S. Johnston, Phys. Rev. B **94**, 235126 (2016).
[38] P. Sémon, K. Haule, and G. Kotliar, Phys. Rev. B **95**, 195115 (2017).
[39] Y. M. Vilk and A.-M. S. Tremblay, J. Phys. I **7**, 1309 (1997).
[40] C. Putzke, A. I. Coldea, I. Guillamón, D. Vignolles, A. McCollam, D. LeBoeuf, M. D. Watson, I. I. Mazin, S. Kasahara, T. Terashima, T. Shibauchi, Y. Matsuda, and A. Carrington, Phys. Rev. Lett. **108**, 047002 (2012).
[41] I. Morozov, A. Boltalin, O. Volkova, A. Vasiliev, O. Kataeva, U. Stockert, M. Abdel-Hafiez, D. Bombor, A. Bachmann, L. Harnagea, M. Fuchs, H.-J. Grafe, G. Behr, R. Klingeler, S. Borisenko, C. Hess, S. Wurmehl, and B. Büchner, Cryst. Growth Des. **10**, 4428 (2010).
[42] J. P. Perdew, K. Burke, and M. Ernzerhof, Phys. Rev. Lett. **77**, 3865 (1996).
[43] P. Blaha, K. Schwarz, G. K. H. Madsen, D. Kvasnicka, and J. Luitz, *WIEN2k: An Augmented Plane Wave plus Local Orbitals Program for Calculating Crystal Properties* (Vienna University of Technology, Vienna, 2001).
[44] A. A. Mostofi, J. R. Yates, G. Pizzi, Y.-S. Lee, I. Souza, D. Vanderbilt, and N. Marzari, Comput. Phys. Commun. **185**, 2309 (2014).
[45] See Supplemental Material at http://link.aps.org/supplemental/10.1103/PhysRevLett.123.256401 for further information on the model, numerical details, the temperature dependence, and the comparison to DMFT, which includes Refs. [15,21,25,39,43,44,46–48].
[46] T. Miyake, K. Nakamura, R. Arita, and M. Imada, J. Phys. Soc. Jpn. **79**, 044705 (2010).
[47] R. Levy, J. LeBlanc, and E. Gull, Comput. Phys. Commun. **215**, 149 (2017).
[48] A. Gaenko, A. Antipov, G. Carcassi, T. Chen, X. Chen, Q. Dong, L. Gamper, J. Gukelberger, R. Igarashi, S. Iskakov, M. Könz, J. LeBlanc, R. Levy, P. Ma, J. Paki, H. Shinaoka, S. Todo, M. Troyer, and E. Gull, Comput. Phys. Commun. **213**, 235 (2017).
[49] H. Jiang, R. I. Gómez-Abal, X.-Z. Li, C. Meisenbichler, C. Ambrosch-Draxl, and M. Scheffler, Comput. Phys. Commun. **184**, 348 (2013).
[50] P. C. Martin and J. Schwinger, Phys. Rev. **115**, 1342 (1959).
[51] G. Baym, Phys. Rev. **127**, 1391 (1962).
[52] S. Arya, P. V. Sriluckshmy, S. R. Hassan, and A.-M. S. Tremblay, Phys. Rev. B **92**, 045111 (2015).
[53] H. Aizawa, K. Kuroki, and J.-i. Yamada, Phys. Rev. B **92**, 155108 (2015).
[54] K. Zantout, M. Altmeyer, S. Backes, and R. Valentí, Phys. Rev. B **97**, 014530 (2018).
[55] T. Mertz, K. Zantout, and R. Valentí, Phys. Rev. B **98**, 235105 (2018).
[56] H. Aizawa and K. Kuroki, Phys. Rev. B **97**, 104507 (2018).
[57] K. Nishiguchi, S. Teranishi, K. Kusakabe, and H. Aoki, Phys. Rev. B **98**, 174508 (2018).
[58] B. Davoudi and A.-M. S. Tremblay, Phys. Rev. B **74**, 035113 (2006).
[59] H. Miyahara, R. Arita, and H. Ikeda, Phys. Rev. B **87**, 045113 (2013).
[60] A.-M. S. Tremblay, Two-particle-self-consistent approach for the Hubbard model, in *Strongly Correlated Systems: Theoretical Methods*, edited by A. Avella and F. Mancini (Springer-Verlag, Berlin, 2012), pp. 409–453.
[61] B. Kyung, J.-S. Landry, and A.-M. S. Tremblay, Phys. Rev. B **68**, 174502 (2003).
[62] D. Ogura and K. Kuroki, Phys. Rev. B **92**, 144511 (2015).
[63] Y. S. Kushnirenko, D. V. Evtushinsky, T. K. Kim, I. V. Morozov, S. Wurmehl, S. Aswartham, A. V. Chubukov, and S. V. Borisenko, arXiv:1810.04446.

Correction: A minor error in Eq. (5) has been fixed.